

A FULL-SCALE MEASUREMENT OF WIND ACTIONS AND EFFECTS ON A SEA-CROSSING BRIDGE

Yi Zhou¹, Limin Sun^{2,*} and Mowen Xie¹

1. *University of Science & Technology Beijing, Department of Civil Engineering, Beijing, China; zhouyi@ustb.edu.cn (Y. Z.); mowenxie@ustb.edu.cn (M. X.)*
 2. *State Key Laboratory of Disaster Reduction in Civil Engineering, Tongji University, Shanghai, China; lmsun@tongji.edu.cn*
- * Corresponding Author

ABSTRACT

Wind loading is critical for the large-span and light-weight structures, and field measurement is the most effective way to evaluate the wind resistance performance of a specific structure. This study investigates the wind characteristics and wind-induced vibration on a sea-crossing bridge in China, namely Donghai Bridge, based on up to six years of monitoring data. It is found that: (1) there exists obvious discrepancy between the measured wind field parameters and the values suggested by the design code; and the wind records at the bridge site is easily interfered by the bridge structure itself, which should be considered in interpreting the measurements and designing structural health monitoring systems (SHMS); (2) for strong winds with high non-stationarity, a shorter averaging time than 10-min is preferable to obtain more stable turbulent wind characteristics; (3) the root mean square (RMS) of the wind-induced acceleration of the girder may increase in an approximately quadratic curve relationship with the mean wind speed; and (4) compared to traffic load, the wind dominates the girder's lateral vibration amplitude, while the heavy-load traffic might exert more influence on the girder's vertical and torsional vibrations than the high winds. This study provides field evidence for the wind-resistant design and evaluation of bridges in similar operational conditions.

KEYWORDS

Sea-crossing bridge, Wind field, Wind-induced vibration, Structural health monitoring

1. INTRODUCTION

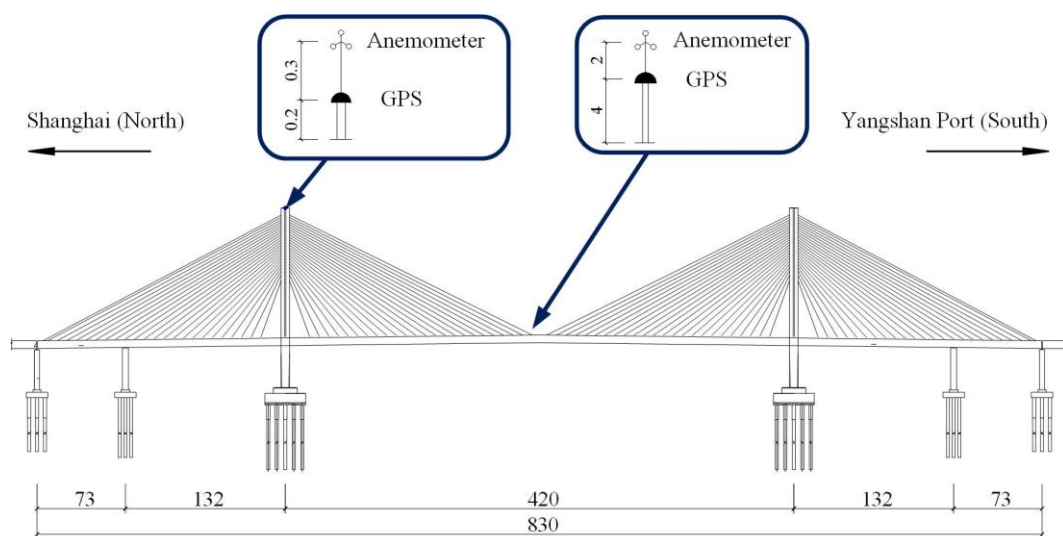
Wind is one of critical loads on large-span and light-weight structures. As the new span record continues to refresh, wind resistance performance of bridges is becoming more and more important. With the development of the structural health monitoring (SHM) technology, many long-span bridges around the world are equipped with structural health monitoring systems (SHMS) to monitor the wind fields on site and the wind-induced responses of structures [1]. Compared with wind tunnel experiments and numerical simulation, field measurement is a more straightforward and effective way to determine the wind-induced responses of the real bridges under the real wind loading. In recent years, the SHM-based researches on wind resistance of bridges have attracted an increasing amount of attention. Case studies include the Tsing Ma Suspension Bridge[2], Runyang Suspension Bridge [3], Sutong Bridge [4], Dongting Lake Bridge [5], Xihoumen Suspension Bridge [6-7], Hangzhou Jiubao Bridge [8], Humber Bridge [9], Akashi Kaikyo Bridge [10], Hakucho Bridge [11], Fred Hartman Bridge [12], and so on.

Each bridge has its own structural configuration and wind field characteristics. As a result, the field observation of wind effects may vary greatly among different bridges, and thus separate

studies are required for individual cases. Based on six years of monitoring data from Donghai Bridge in China, the authors investigated the wind actions and effects on this famous sea-crossing bridge. With a total length of 32.5 km, Donghai Bridge is a super infrastructure which links Shanghai City and the Yangshan Deepwater Container Port. It is located in the typhoon-prone area of the northwestern Pacific Ocean, so the severe wind field is remarkably distinct from the inland bridges. Meanwhile, 80% of the vehicles traversing the bridge are heavy-load container trucks, resulting in a higher level of traffic load than ordinary highway bridges. Hence, both the dynamic effects of high winds and heavy-load traffic are significant on this bridge. The unique environmental and operational conditions make the full-scale measurement research on Donghai Bridge extremely valuable.

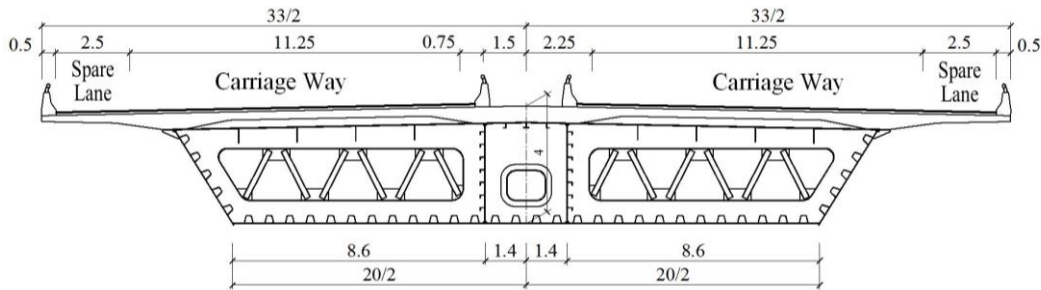
In order to support the bridge management and maintenance, an advanced SHMS was installed on Donghai Bridge in 2006. The majority of sensors are deployed on the main navigational opening (hereinafter referred to as Donghai Bridge for brevity), which is a twin-pylon cable-stayed bridge with a three-cell, steel-concrete composite box girder (Figure 1). There are two anemometers in the monitoring system, one in the mid-span of the girder and the other on the top of the north tower (Figure 1). They can measure wind speed and direction in the horizontal plane with a wind speed range of 0.4 m/s–75 m/s, and have a sampling frequency of 1 Hz. The elevations of the two anemometers are respectively 159.50 m and 58.15 m above the sea level incorporating the sensor’s masts. The vast amount of monitoring data recorded by them provides a solid basis for this study.

The rest of this paper consists of three parts. Section 2 discusses the statistical characteristics of the on-site wind field from 2007–2012. The measured parameters are compared with the suggested values in China’s “Wind-Resistant Design Specification for Highway Bridges” [13] (hereinafter referred to as the Code) or the assumed values in the design stage [14], with an attempt to feedback the design assumptions of Donghai Bridge. Section 3 deliberates on the wind-induced acceleration of the girder, and compares the dynamic effects of strong wind and heavy-load traffic on the bridge vibration. The findings would provide reference information for the traffic control of Donghai Bridge under strong winds, and also benefit the wind-resistant evaluation of bridges in similar operational conditions. Finally, the summary of this paper is presented in the last part.



(a) Elevation view

Fig. 1 - Donghai Bridge and the anemometers on it (units: m)



(b) Standard cross-section of girder

Fig. 1 - Donghai Bridge and the anemometers on it (units: m)

2. WIND CHARACTERISTICS

The records of wind direction and wind speed over six years are retrieved and processed through the conventional vector decomposition method [15] with 10-min averaging time intervals to obtain 10-min mean wind speed \bar{U} as well as along-wind (longitudinal) and across-wind (transverse) turbulent wind speeds (i.e., u and v , respectively). After excluding outliers in the measurements, the characteristics of mean winds and turbulent winds at the bridge site are computed based on approximately 270,000 10-min data sets from the bridge deck and 230,000 from the top of the tower.

2.1. Wind direction frequency

Figures 2 and 3 show the wind roses of the 10-min mean wind at the bridge deck and at the top of tower for six years respectively. The wind speed groups in the figures are based on the Beaufort wind scale [16] without height modification; and the radial length in the wind rose is proportional to the percentage of the data sets for a given wind speed and direction in the total number of data sets, while the tangential length of the plots is meaningless but just for enhancing visualization. There is a clear difference in the prevailing wind direction between the two measuring points. This might be attributed to the deflection of near-ground wind or, more likely, to the disturbance of wind fields caused by the bridge structure.

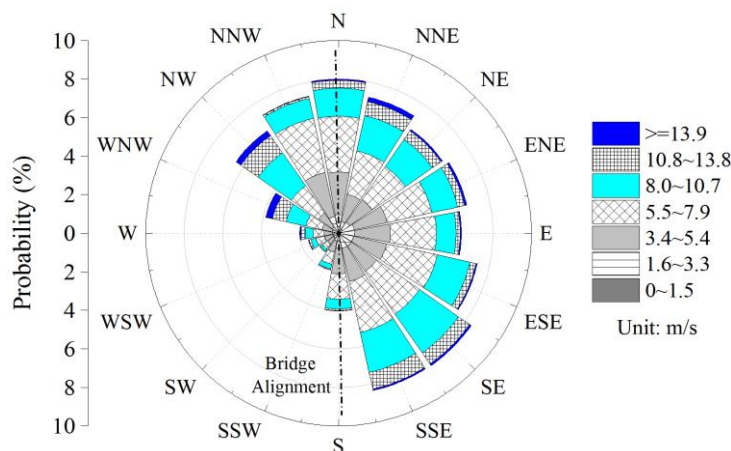


Fig. 2 - Measured wind frequency at the deck

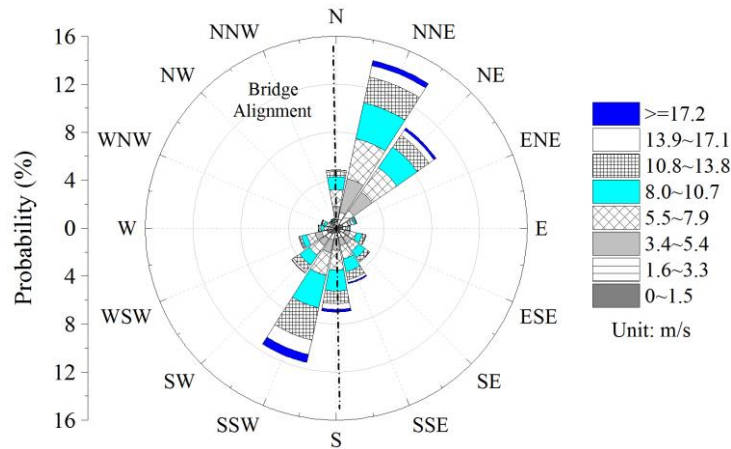


Fig. 3 - Measured wind frequency at the tower top

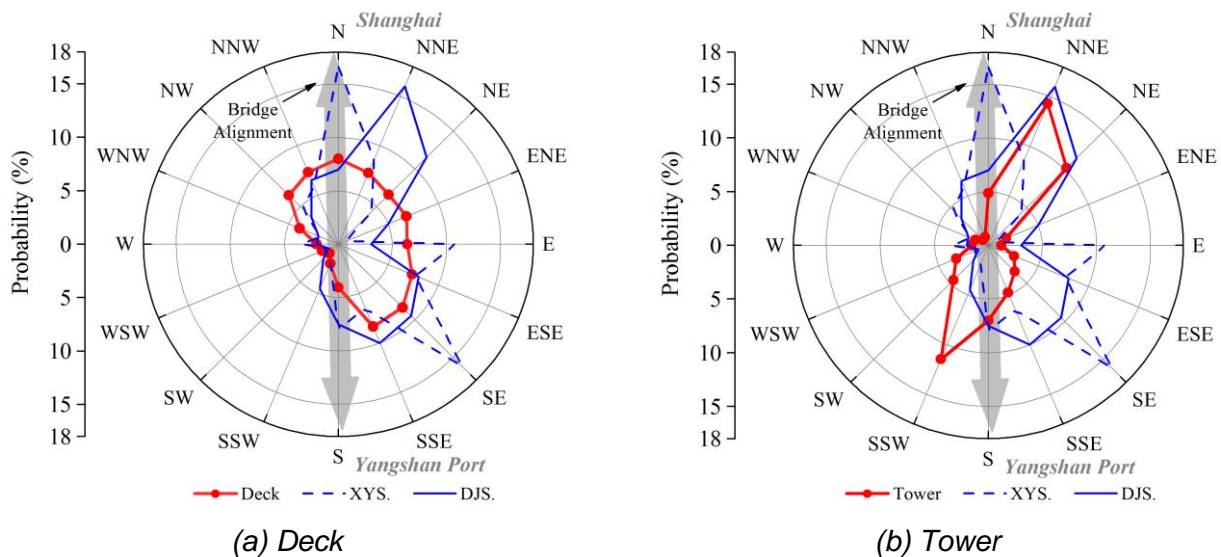


Fig. 4 - Measured wind frequencies versus design values

In the design stage of Donghai Bridge, the wind characteristics at the bridge location was inferred using the wind data from two nearby weather stations in Dajishan (denoted as “DJS”) and Xiaoyangshan (denoted as “XYS”), which are approximately 21 km and 12 km away from the bridge, respectively. As Figure 4 shows, the measured wind direction frequencies are also significantly different with those at the DJS and YYS, indicating a weak correlation between the two points 20 km apart in this sea area.

2.2. Mean wind profile

Using the data sets from the tower top and the bridge deck during the periods when both anemometers are normal, the mean wind profile is estimated based on the power-law profile suggested in the Code [13]:

$$\frac{\bar{U}_T}{\bar{U}_D} = \left(\frac{Z_T}{Z_D} \right)^\alpha \tag{1}$$

where, U and Z respectively represent the 10-min mean wind speed and the altitudes of the measuring points, while the subscripts T and D denote the tower top and bridge deck. The estimated average roughness index α is 0.15, which is higher than the design value ($\alpha = 0.10$). Actually, the dispersion of the fitted index α around the averaged value is considerable, which might result from the influence of the bridge structure on the measurements (Figure 5). The most frequent value in Figure 5 is 0.275.

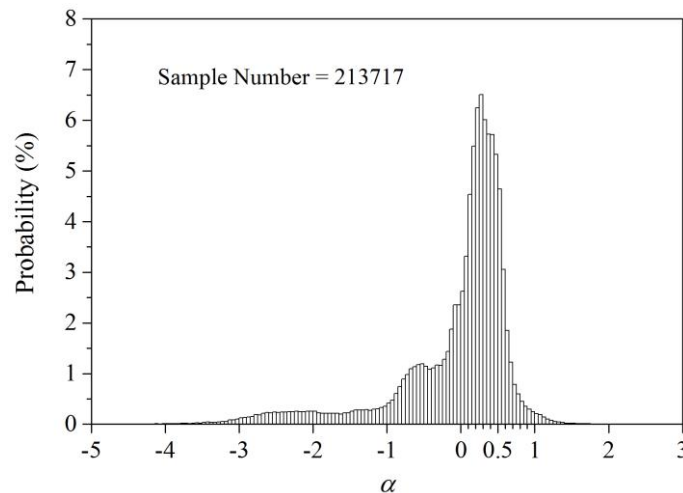


Fig. 5 - Distribution of the fitted roughness index α

2.3. Characteristics of fluctuating winds

Turbulence intensity and integral length scale are calculated to characterize the wind pulsation. Considering the girder is of more interest for structural evaluation, only the measurement at the bridge deck is taken into account here. The average values of the turbulence intensities for longitudinal (along-wind) and transverse (across-wind) components are $I_u = 13.8\%$ and $I_v = 14.6\%$, respectively, which are higher than the values suggested in the Code (i.e., $I_u = 11\%$ and $I_v = 0.88I_u = 9.7\%$) at the height of 50–70 m for the open water. Because the distribution patterns of I_u and I_v at the deck height are similar, Figure 6 only shows the distribution of I_u . Moreover, there is a strong correlation between the measured turbulence intensity in the two directions. The ratio of I_v to I_u is approximately 0.868, which is very close to the suggested value of 0.88 in the Code (Figure 7).

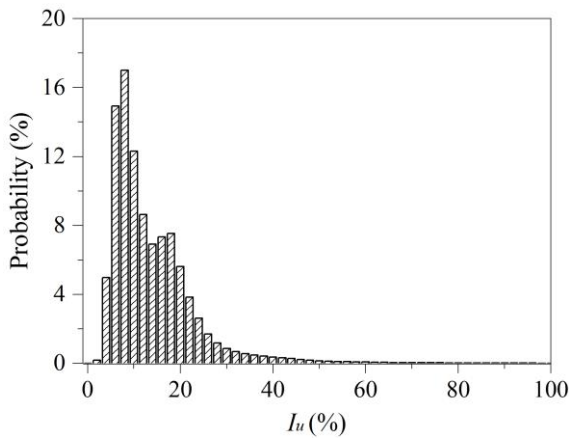


Fig. 6 - Distribution of I_u at the deck level

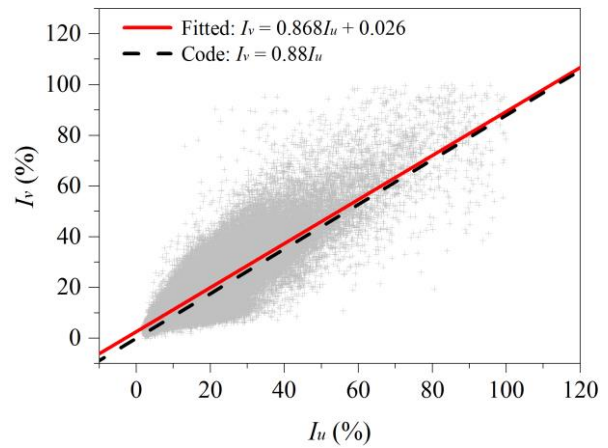


Fig. 7 - Scatter plot of I_u and I_v at the deck level

The turbulent integral length scale reflects the average size of vortices in a fluctuating wind, and we discuss only the integral length scales of longitudinal and transverse turbulent wind in the along-wind direction, i.e. L_u^x and L_v^x . Their distributions at the height of the girder are also close to each other, and Figure 8 displays the case of L_u^x . The measured averages of L_u^x and L_v^x are 89.08 m and 53.09 m, respectively, both of which are smaller than the values of $L_u^x=120$ m and $L_v^x=60$ m suggested in the Code. Together with the aforementioned turbulence intensity observations, the winds at the deck level of the Donghai Bridge have a lower stationarity and stronger turbulence than the suggestions in the Code.

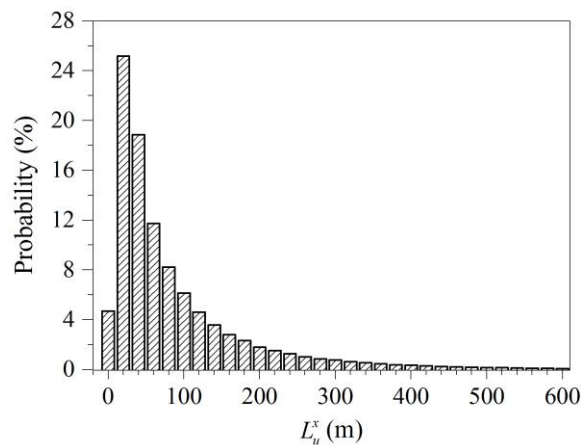


Fig. 8 - Distribution of L_u^x at the deck level

In addition, the variation of wind characteristics with the wind direction is further investigated. The average values of the deck-level I_u , I_v , L_u^x , and L_v^x in different directions are illustrated in Figures 9 and 10. It is noted that a higher turbulence intensity and a smaller integral length scale are observed in the NS direction, indicating the winds along the bridge axis fluctuate more than those in other directions. This probably results from the disturbance of the airflow by the bridge structure.

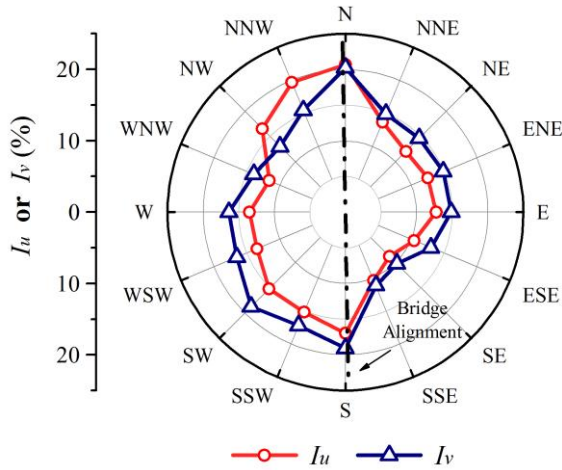


Fig. 9 - Changes in I_u and I_v with wind direction

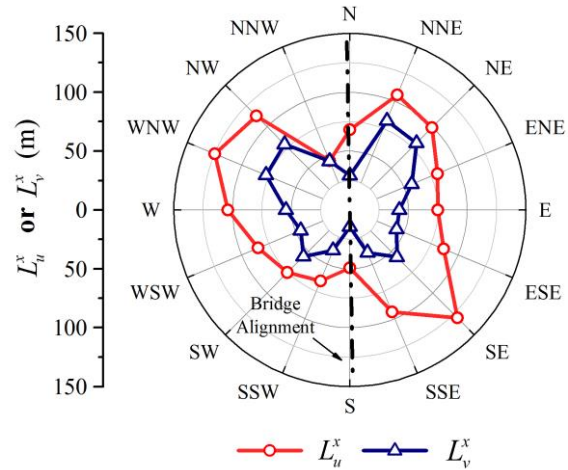


Fig. 10 - Changes in L_u^x and L_v^x with wind direction

2.4. Characteristics of strong winds

The strong wind characteristics at the Donghai Bridge are explored based on five typhoon events (i.e. Whipa, Krosa, Muifa, Haikui, and Bolaven) and a severe convective weather event on August 22, 2008 (denoted as the 8-22 storm). All the six events have an instantaneous wind speed exceeding 25 m/s. Although the 10-min mean wind speed of strong winds are considerably higher than the general winds, however, the turbulence intensity and integral length scale do not show any quantitative pattern.

Actually, due to the increase of non-stationarity, a 10-min averaging duration for wind field analysis may overestimate the turbulent characteristics of strong wind events, and thus a shorter averaging duration is preferable. The 8-22 storm is taken as an example to explicate this issue in Figure 11. When the averaging time interval decreases from 10-min to 1-min, the mean wind speed and direction become closer to the original measurements, and the slowly time-varying trend components in turbulent winds reduce accordingly. The reduction of the low-frequency components will decrease the standard deviation σ_u and the autocorrelation function $R_u(\tau)$ of the turbulent wind, and thereby further reduce the turbulent parameters I_u and L_u^x , which depend on σ_u and $R_u(\tau)$ respectively, as shown in Figure 11. Additionally, the “bump” on the I_u curves at 17:49 in Figure 11 arises because the 1-min mean wind speed \bar{U} , which is the denominator of the calculation formulas $I_u = \sigma_u / \bar{U}$, is close to zero.

Utilizing the data sets during periods with a 10-min mean wind speed higher than 20 m/s, Table 1 compares the 10-min and 1-min averaged turbulent characteristics of the six strong wind events. The parameters calculated based on 1-min time intervals are not only smaller than those with 10-min averaging intervals, but also vary less among different strong winds. Except for the 8-22 storm, the relative reduction of I_u and L_u^x are approximately 20% and 65% respectively, as the averaging time interval decreases from 10-min to 1-min.

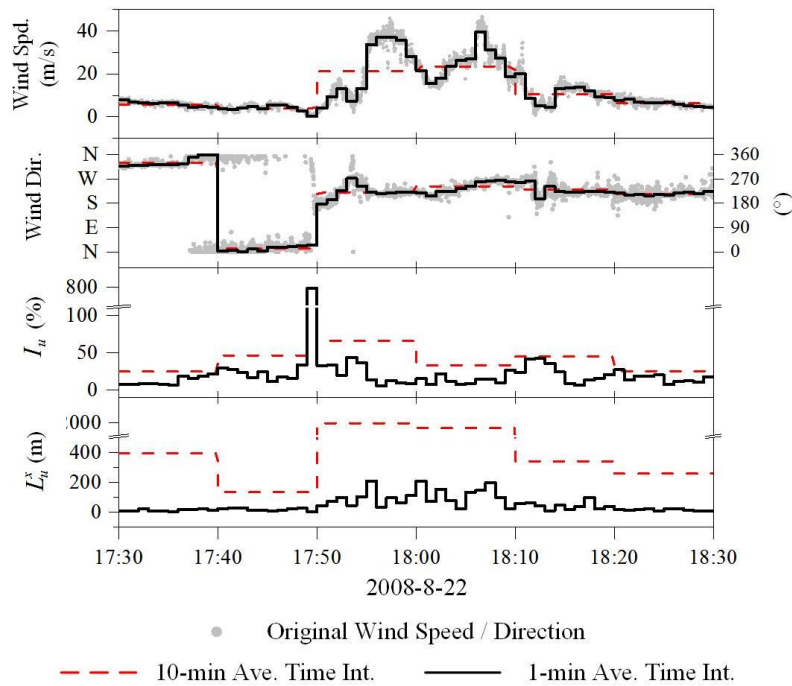


Fig. 11 - Comparison of the wind characteristics during the 8-22 storm using different averaging time intervals

Tab. 1 - Strong wind characteristics calculated using different averaging time intervals

	I_u (%)			L_u^x (m)		
	10-min (1)	1-min (2)	(3) = (2)/(1)	10-min (4)	1-min (5)	(6) = (5)/(4)
Wipha	8.00	6.37	0.796	184.46	68.13	0.369
Krosa	8.53	6.68	0.783	365.92	71.30	0.195
8-22 Storm	49.52	11.98	0.242	1638.98	111.16	0.068
Muifa	10.41	8.51	0.817	334.23	73.14	0.219
Haikui	16.58	15.06	0.908	135.82	69.83	0.514
Bolaven	10.29	7.85	0.763	255.16	91.39	0.358

3. WIND EFFECTS

This section focuses on the wind-induced vertical acceleration \ddot{V} , lateral acceleration \ddot{H} , and torsional (angular) acceleration $\ddot{\alpha}$ at the mid-span section of the girder of Donghai Bridge. Usually, the dynamic effects of the wind and traffic loading are mixed up under operation of a bridge. Fortunately, over the period 2007–2012, Donghai Bridge was once closed to traffic during typhoons Krosa, Muifa, Haikui, and Bolaven, which provided an opportunity for us to investigate the wind effects separately. Thus, these typhoon events were selected for detailed study.

3.1. Structural vibration during high winds

According to the monitoring data recorded during bridge closure for the three typhoon events, i.e. Krosa, Muifa, and Bolaven, Figure 12 shows the correlation of the root mean square (RMS) of the vertical acceleration \ddot{v} and the absolute values of the 10-min mean speed of the orthogonal crosswind (projection of the wind speed perpendicular to the bridge axis, with the positive direction of the wind from west to east). Although the girder's vertical acceleration does not approach zero in a low wind speed, however, there exists a roughly quadratic curve relation between them when the crosswind speed exceeds 13 m/s. This may be attributed to the fact that the wind pressure is proportional to the square of the wind speed. Similar observations of the quadratic curve relation may also be found in the torsional vibration of the girder. But for the most violent typhoon during the period 2007–2012, i.e. Haikui, the acceleration RMS does not indicate any qualitative trend with the increasing wind speed, as the data points in Figure 13 is highly scattered. This finding demonstrates the complexity of the aerodynamic effects, and it is also probably because the wind measuring point at the deck is so limited that it did not depict the severe wind field correctly during Haikui.

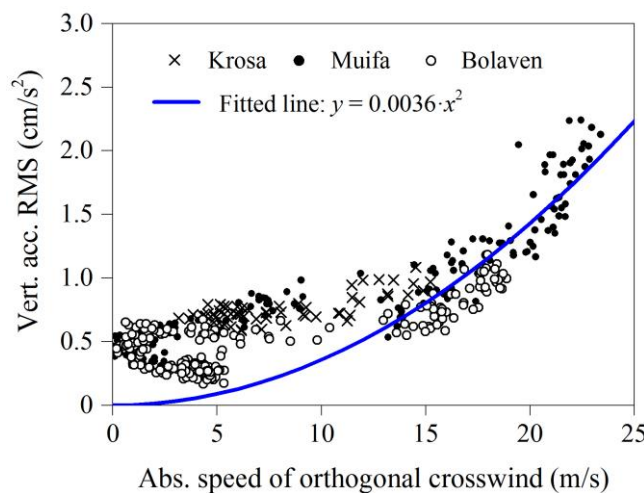


Fig. 12 - Vertical acceleration RMS at mid-span versus wind speed during bridge closure

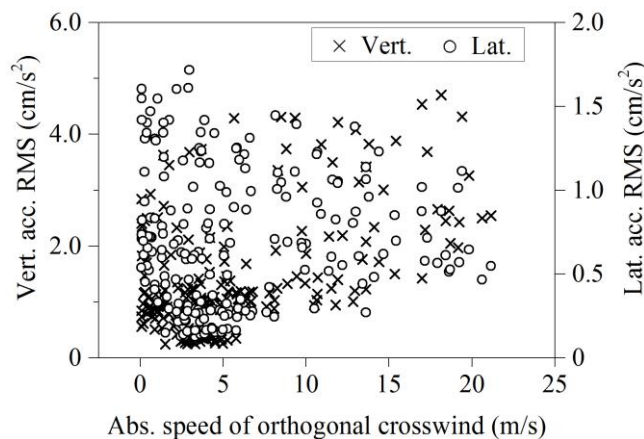


Fig. 13 - Acceleration RMS at mid-span versus wind speed during the Haikui typhoon event

3.2. Comparison between high wind and traffic effects

As China's first offshore sea-crossing bridge with the majority traffic being container trucks, Donghai Bridge has a unique operational condition and is suitable to compare the dynamic effects of high winds and heavy-load traffic on vibration of the girder. Figure 14 shows the evolution of the mid-span acceleration responses during the typhoon Haikui. The acceleration responses in the bridge closure period are dramatically different from the normal traffic period. Clearly, both high winds and heavy-load traffic have a non-negligible impact on the girder vibration.

Table 2 further compares the instantaneous maximum acceleration at mid-span of Donghai Bridge in two different periods: (1) during the bridge closure periods of four typhoon events, when there is the presence of high winds but without traffic load and (2) during normal traffic periods, when there is the absence of high winds but with traffic load. It can be seen from Figure 14 and Table 2, the traffic load is the dominant factor for the vertical and torsional vibration of the girder of Donghai Bridge, because only such an extremely strong typhoon as Haikui can excite the vertical/torsional acceleration to the same level as the traffic load. However, the dominant factor for the lateral vibration of girder is the wind load. The lateral acceleration amplitude in typhoon events is equal to several times that induced by the traffic load, which is understandable for the lateral vibration not being coincidental with the principal acting direction of the traffic on bridges.

Actually, the sensitivity of the structural vertical/torsional vibration to the wind and traffic load depends on the structural configuration and the level of traffic loading. For the Donghai Bridge, the heavy-load traffic dominates the vertical vibration, so the vertical acceleration RMS at the mid-span has a quite weak correlation with the mean wind speed, as shown in Figure 15(a). But for the Shanghai Yangtze River Bridge, a 730 m central span cable-stayed bridge, the vertical/torsional vibration is still dominated by the wind load. This is indicated by Figure 15(b), where a high acceleration RMS almost corresponds to the high wind periods, and the data points can also be fitted by a quadratic curve like Figure 12. It should be noted that the Shanghai Yangtze River Bridge has lower natural frequencies and thus more sensible to the wind action than the Donghai Bridge; also, it undertakes a conventional highway load, not the heavy-load container trucks. These might be the reasons why the vibration of the two bridges have different sensitivity to the wind and traffic load.

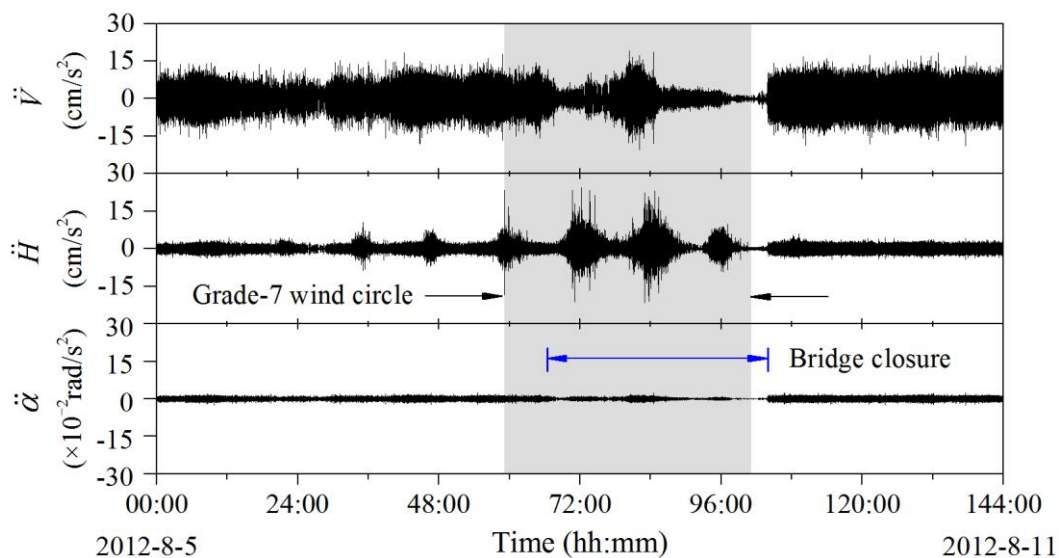


Fig. 14 - Acceleration responses at mid-span during the Haikui typhoon event

Tab. 2 - Maximum acceleration at mid-span between the bridge closure and post-typhoon periods

	Vertical maximum acceleration (cm/s ²)		Lateral maximum acceleration (cm/s ²)	
	During bridge closed (wind dominates)	After typhoons (traffic dominates)	During bridge closed (wind dominates)	After typhoons (traffic dominates)
Krosa	5.23	17.55	28.17	3.85
Muifa	9.18	16.73	12.03	4.95
Haikui	19.02	18.31	24.55	5.98
Bolaven	5.05	20.06	10.26	4.93

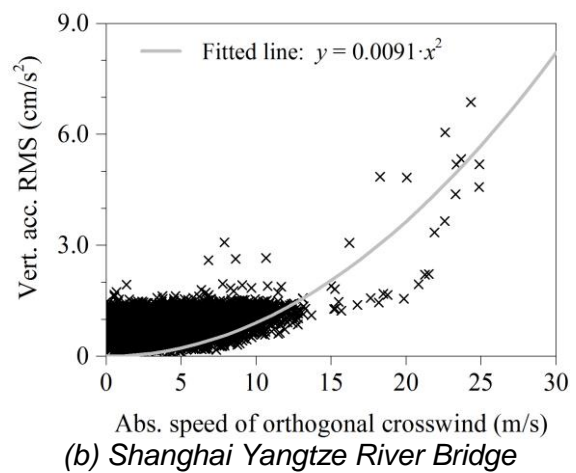
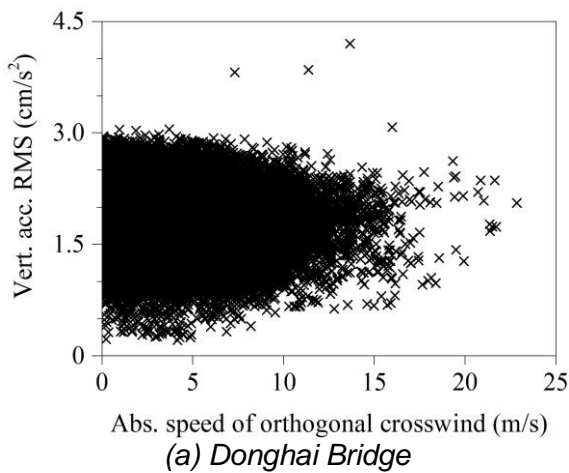


Fig. 15 - Scatter plots of vertical acceleration RMS at mid-span versus wind speed

4. CONCLUSION

The present study discusses the wind field characteristics and the wind-induced vibration responses for a sea-crossing bridge based on the six years of SHM data. In order to validate the design assumptions and understand the structural behaviours, we made a valuable comparison in terms of the measured and assumed wind parameters and also compared the respective contributions of high wind and traffic to the bridge vibration. The following conclusions are drawn:

(1) There exists obvious discrepancy between the measured wind parameters and the values suggested by the design Code, so it is necessary to feedback the design assumptions through the field monitoring. The wind records at the bridge site is easily interfered by the bridge structure itself, which should be considered in interpreting the measurements and designing SHMS.

(2) For strong winds with high non-stationarity, it is preferable to adopt a shorter averaging time than 10-min to calculate turbulent wind parameters. The turbulent characteristics of strong winds over 1-min time intervals are remarkably smaller and vary less among different strong winds than those over 10-min time intervals.

(3) The field measurement demonstrates the complexity of the structural vibrations induced by wind, and the RMS of wind-induced acceleration of the girder may have approximately a quadratic curve relationship with the mean wind speed.

(4) Compared to traffic load, the wind dominates the girder's lateral vibration amplitude, whereas the heavy-load traffic may exert more influence on the girder's vertical and torsional vibrations than the high winds, such as the case in Donghai Bridge.

This study provides field evidence for the wind-resistant design and evaluation of bridges in similar operational conditions.

ACKNOWLEDGEMENTS

The authors express their profound appreciation for the financial support provided by the projects of the National Natural Science Foundation of China (Grant No.: 51608034), the China Postdoctoral Science Foundation (Grant No.: 2016M600925), the Fundamental Research Funds for the Central Universities (Grant No.: FRF-TP-16-012A1), and the National Basic Research Program of China (973 Program, Grant No.: 2013CB036305). We also would like to thank the Shanghai Donghai Bridge Management Co.,Ltd. and the Shanghai Just One Technology Development Co.,Ltd. for the great assistance.

REFERENCES

- [1] Xu, Y., 2013. Wind Effects on Cable-supported Bridges (John Wiley & Sons, Singapore)
- [2] Xu Y., Guo W., Chen J., et al., 2007. Dynamic Response of Suspension Bridge to Typhoon and Trains. I: Field Measurement Results. *Journal of Structural Engineering*, vol. 133(1): 3-11
- [3] Wang H., Guo T., Tao T., et al., 2016. Study on Wind Characteristics of Runyang Suspension Bridge Based on Long-term Monitored Data. *International Journal of Structural Stability and Dynamics*, vol. 16: 1640019
- [4] Wang H., Li A., Niu J., et al., 2013. Long-term Monitoring of Wind Characteristics at Sutong Bridge Site. *Journal of Wind Engineering and Industrial Aerodynamics*, vol. 115(0): 39-47
- [5] Ni Y., Wang X., Chen Z., et al., 2007. Field Observations of Rain-Wind-Induced Cable Vibration in Cable-Stayed Dongting Lake Bridge. *Journal of Wind Engineering and Industrial Aerodynamics*, vol. 95(5): 303-328
- [6] Liu M., Liao H., Li M., et al., 2012. Long-term Field Measurement and Analysis of the Natural Wind Characteristics at the Site of Xi-Hou-Men Bridge. *Journal of Zhejiang University Science A*, vol. 13(3): 197-207
- [7] Li H., Laima S., Zhang Q., et al., 2014. Field Monitoring and Validation of Vortex-induced Vibrations of a Long-Span Suspension Bridge. *Journal of Wind Engineering and Industrial Aerodynamics*, vol. 124(0): 54-67
- [8] Chen B., Wang X., Sun D., et al., 2014. Field Measurement of Near-ground Wind Characteristics of Typhoon Haikui at Site of Jiubao Bridge. *Bridge Construction*, vol. 44(4): 34-39 (in Chinese)
- [9] Brownjohn J., Zasso A., Stephen G., et al., 1995. Analysis of Experimental Data from Wind-induced Response of a Long Span Bridge. *Journal of Wind Engineering and Industrial Aerodynamics*, vol. 54–55(0): 13-24
- [10] Miyata T., Yamada H., Katsuchi H., et al., 2002. Full-scale Measurement of Akashi–Kaikyo Bridge During Typhoon. *Journal of Wind Engineering and Industrial Aerodynamics*, vol. 90(12–15): 1517-1527
- [11] Abe M., Fujino Y., Yanagihara M., et al., 2000. Monitoring of Hakucho Suspension Bridge by Ambient Vibration Measurement. In: *Proceedings of SPIE*, Volume 3995 (SPIE, Bellingham)
- [12] Joseph A., Nicholas P., 2000. A Comparison of Full-scale Measurements of Stay Cable Vibration. In: *Proceedings of Structures Congress 2000* (ASCE, Reston)
- [13] Ministry of Transport of the People's Republic of China, 2004. Wind-resistant Design Specification for Highway Bridges (JTG/T D60-01—2004). Beijing: China Communications Press (in Chinese)
- [14] Zhu Z., 2007. Wind-induced Response Analysis for Main Navigation Channel Bridge of the East Sea Bridge. Master Thesis of Tongji University, Shanghai (in Chinese)
- [15] Xu Y., Chen J., 2004. Characterizing Nonstationary Wind Speed Using Empirical Mode Decomposition. *Journal of Structural Engineering*, vol. 130(6): 912-920
- [16] Simiu E, Scanlan R H. *Wind Effects On Structures : Fundamentals and Applications to Design*. 3rd ed. New York: John Wiley & Sons, 1996.